Optimal battery thermal management for electric vehicles with battery degradation minimization

Wu, Yue; Huang, Zhiwu; Li, Dongjun; Li, Heng; Peng, Jun; Stroe, Daniel; Song, Ziyou

Published in:
Applied Energy

DOI (link to publication from Publisher):
10.1016/j.apenergy.2023.122090

Publication date:
2024

Document Version
Early version, also known as pre-print

Optimal battery thermal management for electric vehicles with battery degradation minimization

Yue Wu[1], Zhiwu Huang[1], Dongjun Li[2], Heng Li[3*], Jun Peng[3], Daniel Stroe[4], and Ziyou Song[2,**]
Corresponding author: Heng Li (liheng@csu.edu.cn) and Ziyou Song (ziyou@nus.edu.sg)

[1] *School of Automation, Central South University, Changsha 410075, China*
[2] *Department of Mechanical Engineering, National University of Singapore, Singapore 117575, Singapore*
[3] *School of Computer Science and Engineering, Central South University, Changsha 410075, China*
[4] *Department of Energy Technology, Aalborg University, Aalborg 9220, Denmark*

Abstract

The control of a battery thermal management system (BTMS) is essential for the thermal safety, energy efficiency, and durability of electric vehicles (EVs) in hot weather. To address the battery cooling optimization problem, this paper utilizes dynamic programming (DP) to develop an online rule-based control strategy. Firstly, an electrical-thermal-aging model of the $LiFePO_4$ battery pack is established. A control-oriented onboard BTMS model is proposed and verified under different speed profiles and temperatures. Then in the DP framework, a cost function consisting of battery aging cost and cooling-induced electricity cost is minimized to obtain the optimal compressor power. By exacting three rules "fast cooling, slow cooling, and temperature-maintaining" from the DP result, a near-optimal rule-based cooling strategy, which uses as much regenerative energy as possible to cool the battery pack, is proposed for online execution. Simulation results show that the proposed online strategy can dramatically improve the driving economy and reduce battery degradation under diverse operation conditions, achieving less than a 2.18% difference in battery loss compared to the offline DP. Recommendations regarding battery cooling under different real-world cases are finally provided.

Keywords: Battery thermal management system; Battery degradation; Electric vehicles; Eco-cooling; Dynamic programming; Economy analysis.

1. Introduction

Benefiting from zero-emission and low operation cost features, electric vehicles (EVs) powered by Li-ion batteries have an increasing penetration rate in the automotive market. However, battery overheating or even thermal runaway [1] still hinders consumer acceptance of EVs, especially in those areas with hot weather [2]. In this context, battery cooling is of vital importance to ensure thermal safety and further improve the driving economy [3]. Battery temperature is actively controlled by the battery thermal management system (BTMS) [4], which requires careful structure designs [5, 6] to improve cooling efficiency and also, well-designed battery cooling control strategies to realize real-time, efficient, and energy-saving cooling performance [7]. The BTMS should be able to regulate the battery temperature and maintain it within a safe range to extend the battery life and improve vehicle performance.

Generally, BTMS can be categorized as active, passive, and hybrid systems [8]. Active BTMSs require an additional energy source (a fan, blower, or pump) to exchange the heat between the battery pack and the thermal conductive media, e.g., air flow or liquid flow. When compared to passive and hybrid BTMSs, active BTMSs well balance the complexity of the cooling structure and cooling performance and are therefore widely applied in commercial EVs [9]. Finite element analysis and computational fluid dynamics are commonly used for precise modeling [10, 11] and structure optimization [12, 13] of active BTMSs. These efforts have contributed significantly to the improvement of heat exchange efficiency and the design of practical BTMSs. With a well-designed active BTMS, meticulous control is critical for BTMS operation where two main issues need to be addressed: (1) A control-oriented model with adequate accuracy and acceptable complexity is required since BTMS control involves

complex refrigerant phase change and coupled electrical-thermal processes [14]; and (2) Considering the coupled electrical-thermal-aging characteristics of batteries [15], operation optimization for battery cooling is needed to simultaneously reduce battery aging [16] and cooling energy consumption from battery pack itself [17, 18].

Extensive studies about control-oriented BTMS modeling have been conducted in recent years. Amini et.al [19] considered a simple constant ratio between the battery cooling rate and BTMS power, and they further developed a polynomial fitting model with acceptable accuracy, where the temperature dynamics of battery, cabin, and evaporator are involved [20]. Similar work can also be found in [21]. To build more accurate models, Park et.al [22] further established a detailed control-oriented BTMS model considering different mass flow rates of the R134a refrigerant and pressure ratios. Kuang et.al [23] considered a high-fidelity heat transfer process and built models for the compressor, condenser, evaporator, chiller, and expansion valve.

Regarding the battery cooling strategy, there have been numerous studies that can be classified into offline optimization methods [21, 23–25] and online optimization methods, based on, for example, look-up tables [24], fuzzy PID [25], and model predictive control (MPC) [19–22, 26, 27].

In terms of offline cooling strategies, a hierarchical and iterative dynamic programming (HIDP) scheme [21] was proposed to provide the optimal battery temperature trajectory so that an MPC can track and minimize cooling power. Similarly, Zhao et.al [25] proposed a fuzzy PID to track the optimal temperature trajectories from dynamic programming (DP), where the optimal battery target temperature is calculated considering weather conditions, passenger characteristics, and battery conditions. Kuang et. al [23] proposed a genetic algorithm method to explicitly minimize the battery capacity loss (i.e., battery degradation) and cooling power, where different weight coefficients were discussed carefully. Bauer et.al [24] developed an offline Pontryagin's maximum principle (PMP)-based battery cooling strategy to minimize the consumed battery energy and battery temperature tracking error (then a look-up table based on the PMP is designed for online execution). The above offline battery cooling optimization methods all require EVs' entire traction power/speed profile as a priori and suffer from heavy computation burdens, which are difficult to use in practice.

To realize online cooling optimization, MPC can be a promising online optimization method leveraging future information [28] and has been widely investigated. A hierarchical MPC framework is proposed for cabin/battery thermal management optimization in EV [19] and hybrid electric vehicles (HEVs) [20]. Park et.al [22, 26] developed a stochastic MPC to handle uncertainties of future information by designing a stochastic model of future heat generation. In these studies, the cooling power and battery temperature tracking error are optimized. Xie et.al [27] proposed a battery cooling MPC method to optimize the battery temperature tracking error, coolant flow rate, and the change rate of coolant flow.

Despite the above-related studies, there are still several issues to be resolved. To the best of our knowledge, (1) A control-oriented BTMS model that is effective under different working conditions, e.g., EV velocity, environment temperature, and BTMS parameters, is still missing in the available literature; (2) An online battery cooling optimization method that minimizes the battery capacity degradation has not been reported yet; (3) From the perspective of battery degradation and driving economy, how to cool the battery under different conditions is still an open problem.

To address the challenges, this paper presents a comprehensive investigation of EV battery cooling optimization based on dynamic programming. Firstly, a control-oriented BTMS model is established and verified under different working conditions. Then an offline DP-based battery cooling strategy is proposed to minimize the costs of battery capacity degradation and battery cooling. By analyzing the DP results under various driving conditions (urban, suburban, and highway), three rules are extracted to construct a near-optimal rule-based cooling strategy for online implementation. Finally, a quantitative analysis and comparison with existing studies are conducted to indicate the superiority and optimality of the proposed online strategy, together with a comprehensive analysis of the driving economy under versatile conditions. An intuitive comparison between the existing literature [19–27] and this paper is presented in Table 1. Compared with existing studies, the contributions of this paper can be summarized below.

1. A control-oriented BTMS model, which has high accuracy under wide ranges of EV velocity (0∼120km/h), environmental temperature (26∼40°C), and mass flow rate of the coolant (0.14∼0.22kg/s), is established through orthogonal experiments and data fitting.

2. The proposed online cooling strategy, which can minimize battery capacity loss and cooling energy by leveraging regenerative power, is verified to achieve near-optimal performance with ease of implementation in EV applications when compared to DP results.

Table 1: Comparison of the reviewed battery cooling studies

Literature	Cooling type	BTMS modeling (cooling rate/power relation)	Model validation under different	Environmental temperature (°C)	Cooling strategy (online/offline)	Optimization objective
Ref. [19]	Liquid+Air	Constant ratio	-	30	Hierarchical MPC (online)	T_{bat} error cooling power
Ref. [20]	Air	Mechanism modeling Polynomial fitting	EV speed/fan speed	30[1]	Hierarchical MPC (online)	T_{bat} error cooling power SoC_{bat} error[2]
Ref. [21]	Air	Mechanism modeling Polynomial fitting	EV speed cooling power	30	HIDP (offline) MPC (online)	T_{bat} error cooling power
Ref. [22]	Liquid	Mechanism modeling Interpolation fitting	coolant mass flow rate compressor speed/torque pressure ratio	30[1]	stochastic MPC (online)	T_{bat} error cooling power
Ref. [23]	Liquid	Mechanism modeling	pressure ratio condenser wind speed refrigerant mass flow rate coolant volume flow rate compressor speed	30	genetic algorithm (offline)	battery degradation cooling power
Ref. [24][3]	-	Constant ratio	-	-30, 60[1]	PMP (offline) lookup table (online)	T_{bat} error cooling/heating power
Ref. [25]	Liquid	Mechanism modeling	EV speed	33[1]	DP (offline) fuzzy PID (online)	T_{bat} error cooling power
Ref. [26]	Liquid	Mechanism modeling Interpolation fitting	coolant mass flow rate compressor speed/torque pressure ratio	28∼34[1]	stochastic DP (offline) stochastic MPC (online)	T_{bat} error cooling power
Ref. [27]	Liquid	Mechanism modeling	coolant mass flow rate	15∼30	MPC (online)	T_{bat} error coolant flow rate coolant flow change rate
This work	Liquid	Mechanism modeling Interpolation fitting	EV speed coolant mass flow rate environmental temperature	26∼40	DP (offline) rule (online)	battery degradation cooling power

[1] The environmental temperature is not explicitly mentioned, the initial battery temperature is listed.
[2] Ref. [20] studied both thermal management and power allocation of HEVs, thus the battery SoC is planned.
[3] Ref. [24] studied both battery heating and cooling.

3. A comprehensive and quantitative driving economy analysis is presented to explore the performance of the proposed cooling strategy under versatile operating conditions, i.e., driving conditions, environmental temperatures, and BTMS parameters. Recommendations for battery cooling are then provided.

The remainder of this paper is organized as follows. In Section 2, detailed modeling of the battery pack and BTMS is introduced. Offline DP optimization for battery cooling together with the results are illustrated in Section 3. Analysis of the DP results and the rule-based cooling strategy are proposed in Section 4. Section 5 presents the detailed results and analysis. Conclusions are drawn in Section 6.

2. System Modeling

As shown in Fig. 1, the studied system includes a battery pack as the energy storage system, and the auxiliary load corresponding to the BTMS, which consists of two thermal loops, i.e., the battery cooling loop and the refrigeration loop. The battery cooling power $P_{cooling}$ comes from the electricity consumption of the compressor, the pump, and the fan.

2.1. EV model

The power balance between the battery pack, the BTMS, and the traction system is given as

$$(P_d + P_{cooling})/\eta_{dcac} = P_{bat} \tag{1}$$

where P_d is the traction/braking power, $P_{cooling}$ is the total power of the compressor, the pump, and the fan, η_{dcac} is the inverter efficiency, and P_{bat} is the power of the battery pack. Detailed modeling and parameters of the DC/AC inverter, motor, powertrain, and vehicle dynamics can be found in our previous work [29].

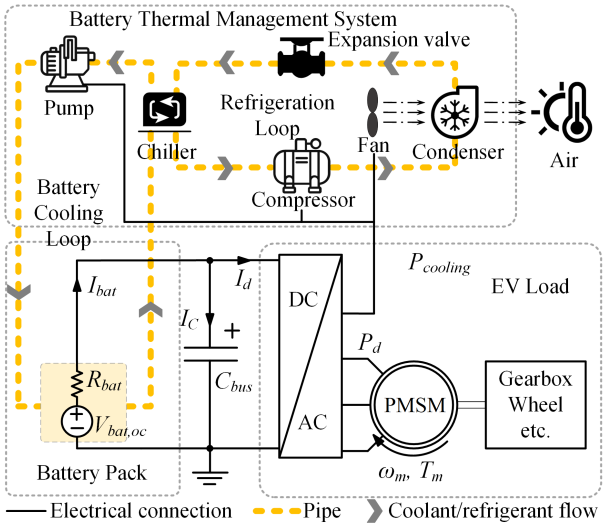

Figure 1: Battery energy storage system, battery thermal management system, and traction load of the electric vehicle.

2.2. Battery electrical model

The *Rint* model is considered for modeling the dynamics of the battery pack. The voltage, power, and state-of-charge (SoC) dynamics are given below:

$$V_{bat} = V_{bat,oc} - I_{bat}R_{bat} \tag{2}$$

$$P_{bat} = V_{bat,oc}I_{bat} - I_{bat}^2R_{bat} \tag{3}$$

$$SoC_{bat,k+1} = SoC_{bat,k} - \frac{I_{bat,k}T_s}{3600Q_{bat}}, \tag{4}$$

where $V_{bat,oc}$ and V_{bat} represent the open-circuit voltage and terminal voltage, I_{bat} denotes the battery current, R_{bat} is the internal resistance, $V_{bat,oc}$ is a function of battery SoC, given in [30], R_{bat} is a function of charging/discharging, SoC, and temperature, provided in [31], and Q_{bat} is the capacity of the battery pack. T_s is the sampling time. Other basic parameters of the $LiFePO_4$ battery cell considered in this work are given in Table 2. In the studied EV, 250-60Ah cells form a 120Ah-412V battery pack [32] (125 in series, 2 in parallel).

Table 2: Parameters of the Li-ion battery

Parameter	Battery (cell)
Capacity	60Ah
Nominal voltage	3.3V
Stored energy	192Wh
Mass	2.5kg
SoC range	[5%,100%]

2.3. Battery aging model

A dynamic capacity degradation model for $LiFePO_4$ batteries [16] is utilized to quantify the battery degradation. Through experimental testing and parameter calibration from 5°C to 45°C [33], the discrete form of this model is provided as

$$\Delta Q_{loss,k} = 9.78 \times 10^{-4} \frac{|I_{bat,k}|T_s}{3600} e^{\left(\frac{-15162+1516C_{rate,k}}{0.849RT_{bat,k}}\right)} Q_{loss,k-1}^{-0.1779} \tag{5}$$

where $\Delta Q_{loss,k}$ is the instantaneous capacity loss (%), R is the gas constant 8.314J/(mol·K), $T_{bat,k}$ is the battery absolute temperature (K), $C_{rate,k}$ is the current rate (i.e., $|I_{bat}|/Q_{bat}$), and T_s denotes the sampling time. Therefore, the incremental capacity reduction $\Delta Q_{loss,k}$ is a non-linear function of $I_{bat,k}$ and $T_{bat,k}$, and it will be directly incorporated in the cost function in this paper.

2.4. Battery thermal model

Heat generation of the battery pack mainly consists of resistance joule heat and reversible entropy heat [34], which are the first term and the second term in Eq. (6).

$$\dot{Q}_{gen} = I_{bat}^2 R_{bat} + I_{bat} T_{bat} \frac{dV_{bat}}{dT_{bat}} \tag{6}$$

where $\frac{dV_{bat}}{dT_{bat}}$ is derived through the entropy potential calibration of the $LiFePO_4$ cell, the detailed results can be found in [31] (positive current denotes discharging). For simplicity, all battery cells are assumed to have the same electrical and thermal parameters, i.e., no temperature variation is considered among cells. Moreover, this study does not distinguish the core temperature and surface temperature of the battery cell, the core temperature can be estimated using the surface temperature as described in [35]. Hence, the battery temperature dynamics can be derived, as shown below [34].

$$\frac{dT_{bat}}{dt} = \frac{\dot{Q}_{gen} - \dot{Q}_{cool}}{N_{cell} C_{cell}} \tag{7}$$

where $N_{cell} = 250$ is the total number of battery cells in the pack, C_{cell} is the thermal capacity of the battery cell, i.e., 2299J/°C, and $\dot{Q}_{cool}$ is the battery cooling rate, determined by the BTMS.

The electrical-thermal-aging coupling relationship of the Li-ion battery is shown in Fig. 2. The battery current I_{bat} is the input of these coupled models, then battery states such as SoC, terminal voltage, heat generation, temperature, and capacity loss are calculated. Battery temperature T_{bat} will be fed back to update the electrical and aging models iteratively and is determined by the environment temperature, heat generation, and cooling rate.

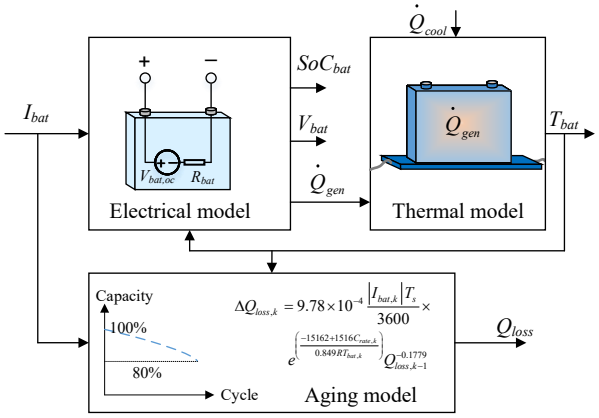

Figure 2: Coupling relationship between battery electrical, thermal, and aging models.

2.5. Battery thermal management system model

Fig. 3 shows the framework and schematic of the studied BTMS, where the colored lines highlight the two thermal loops. The solid line represents the refrigeration loop, and the double solid line represents the battery cooling loop. For the refrigeration loop, driven by the compressor, the refrigerant undergoes several procedures

through the compressor, condenser, expansion valve, and Chiller. It turns into high-pressure superheated vapor from low-pressure superheated vapor through compression, then dissipates heat to ambient air through the condenser with a new state of high-pressure cooled liquid. After the expansion valve, the refrigerant turns into low-pressure mixed liquid and vapor, while the temperature drops due to liquid vaporization. Finally, the mixed refrigerant liquid and vapor absorb heat through the chiller.

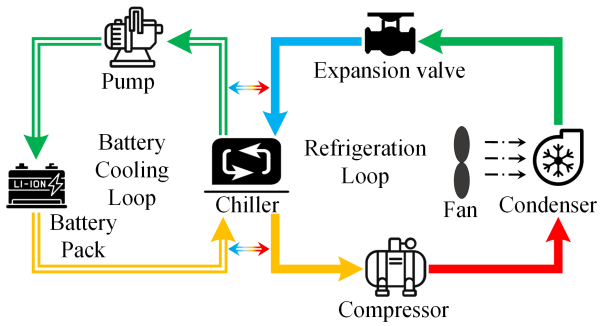

Figure 3: Battery thermal management system. Red, orange, green, and blue represent the temperatures from high to low.

The above processes form a compressed refrigeration cycle of the air-conditioning system [36, 37]. For the battery cooling loop, driven by the pump, the coolant flows into the battery pack to absorb heat generated by the battery pack. Then the heat exchange process between the coolant and refrigerant will occur while the coolant flows into the Chiller. To sum up, the studied BTMS model contains three sub-models: a sub-model describes the relationship between cooling power and consumed energy of BTMS (sub-model I), a sub-model describing the heat exchange between the battery pack and coolant (sub-model II), and a sub-model describing the heat exchange between the coolant and refrigerant in Chiller (sub-model III).

For sub-model I, the total electricity consumption comes from three parts, i.e., pump, fan, and compressor. Considering that the power levels of the pump (less than 50W) and the fan (about 100∼200W) are much lower than the compressor (500∼4500W), we simplify the power calculation by treating the power of the pump and fan as constants to reduce complexity. Therefore, only P_{comp} is considered as the control variable in the studied BTMS. Specifically, the main control strategy for the fan and pump is rule-based, where their real-time power varies according to a preset strategy. According to simulation results in [38], an average power consumption of 200W for the fan and pump is considered. This assumption simplifies the modeling while still capturing the general power characteristics of the fan and pump under typical conditions. For more details about the control strategy of the pump and fan, please refer to [38]. With these considerations, we can express the total power of the BTMS as follows

$$P_{cooling} = P_{comp} + 200. \tag{8}$$

As mentioned above, the compression refrigeration process is a highly nonlinear process, which requires quantities of complicated equations to describe. To reduce calculation burden and model complexity, a model describing the relationship between cooling rate and power consumed by the AC system is fitted by orthogonal simulation experiment data. Data was generated by a vehicle AC system model built into KULI software [36–39], this model was well validated by experimental vehicle data. The model is given as

$$\begin{aligned} \dot{Q}_{cool} = \lambda_1 P_{comp} + \lambda_2 P_{comp}^2 + \lambda_3 T_{clnt,out} + \lambda_4 T_{air}\dot{m}_{air} \\ + \lambda_5 T_{clnt,out}\dot{m}_{clnt} + \lambda_6 \end{aligned} \tag{9}$$

$$\dot{m}_{air} = 0.07065 + 0.00606v \tag{10}$$

where $\dot{Q}_{cool}$ represents the supplied cooling rate (power) to the battery pack from the BTMS, P_{comp} is the compressor electrical power, $T_{clnt,out}$ is the outlet temperature of the coolant, T_{air} is the environment temperature, $\dot{m}_{air}$ denotes the total air mass flow through the condenser, $\dot{m}_{clnt}$ is the mass flow rate of coolant, v is the EV velocity (km/h),

and λ_i are different coefficients determined by T_{air} and $\dot{m}_{clnt}$. Eq.(10) describes the relationship between the air mass flow rate and the EV velocity. In addition, all coefficients λ_i are functions of T_{air} and $\dot{m}_{clnt}$, as shown in Fig. 4. With these fitted coefficients, more than 80% and 97% of the model/experiment data have an error of less than 5% and 10%, respectively, see Fig. 5. More details of the BTMS orthogonal experiment and λ_i values are given in the Appendix.

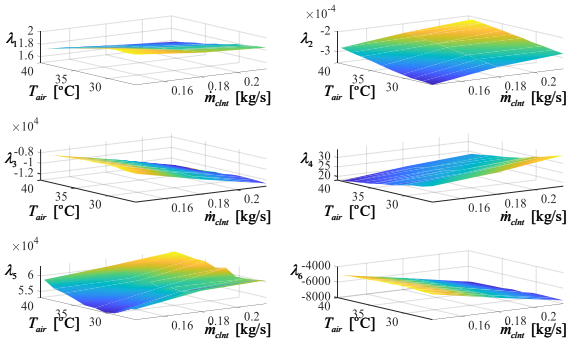

Figure 4: Model fitted coefficients of the BTMS model λ_i.

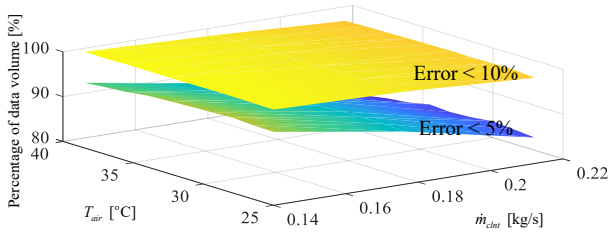

Figure 5: Percentage of data with model error less than 5% and 10%.

The working ranges of the key variables are determined by application scenarios and operation range of each component [36, 38, 40], see Table 3. P_{comp} is the control variable with operation range [500, 4500W]. When P_{comp} is too low, i.e., less than 500W, the compressor has a low rotation speed (less than 500rpm), thereby failing to repress refrigerant and negatively impacting the compressor. As a result, we assume $\dot{Q}_{cool} = 0$ when $P_{comp} < 500$W.

Table 3: Application scope of BTMS orthogonal experiment

Input variables	Value	Unit
Outlet temperature of coolant $T_{clnt,out}$	25∼39	°C
Volumetric flow rate of coolant $\dot{q}_{clnt}$	8∼12	L/min
Ambient air temperature T_{air}	26∼39.5	°C
EV velocity v	0∼120	km/h
Compressor power P_{comp}	500∼4500	W

The following Eqs. (11) and (12) describe the heat exchange process of sub-models II and III of BTMS [22].

$$T_{clnt,out} = (T_{clnt,in} - T_{bat})e^{\frac{-h_{bat}A_{bat}}{\dot{m}_{clnt}c_{clnt}}} + T_{bat} \tag{11}$$

$$T_{clnt,in} = T_{clnt,out} - \frac{\dot{Q}_{cool}}{\dot{m}_{clnt}c_{clnt}} \tag{12}$$

where $T_{clnt,in}$ is the temperature of the coolant inlet, h_{bat} represents the heat transfer coefficient between the battery and the coolant, A_{bat} is the heat transfer area between the battery and the coolant, c_{clnt} denotes the specific heat capacity of the coolant. All the constant parameters of sub-models II and III are listed in Table 4, note that more T_{air}, $\dot{m}_{clnt}$, and A_{bat} parameters are tested in Section 5.

Table 4: Parameter settings of the BTMS

Description and symbol	Value	Unit
Specific heat capacity of coolant c_{clnt}	3330 [22]	J/kg/°C
Heat transfer coefficient between battery/coolant	300 [22]	W/m^2/°C
Mass flow rate of the coolant $\dot{m}_{clnt}$	0.18	kg/s
Heat transfer area between battery/coolant A_{bat}	3.1	m^2
Environment temperature T_{air}	33	°C
Initial temperatures of the coolant inlet $T_{clnt,in}$	33	°C
Initial temperatures of the coolant outlet $T_{clnt,out}$	33	°C

3. Offline optimization of battery thermal management

This section illustrates the offline optimization of battery cooling using DP under typical driving conditions, and the DP results may provide some insightful guidance to design online battery cooling strategies.

3.1. Dynamic programming development

First, we set a target battery temperature of 25°C in the cooling process under hot weather conditions, as generally, there is no need to cool the battery down to a lower temperature for most battery chemistries [8, 41], considering the tradeoff between energy consumption and battery degradation rate [25]. In the DP process, the primary state is the battery temperature T_{bat}, which is discretized into 111 states (with the temperature resolution of about 0.1°C) in the range of $[T_{bat,min}, T_{bat,max}]$, where $T_{bat,min} = 24$°C, $T_{bat,max} = T_{air} + 2$°C. Temperature margins of 1∼2°C are set to ensure all temperatures around 25°C and T_{air} can be considered, i.e., the optimal control variable is available for the query if the battery temperature is slightly below 25°C or above T_{air} in the forward execution. The control variable is the compressor power P_{comp}, which is also divided into 111 discrete states. The backward search procedure of DP on the time domain is shown in Fig. 6, when all discrete states and actions are traversed, an offline table of the Value function is established for the forward execution [42].

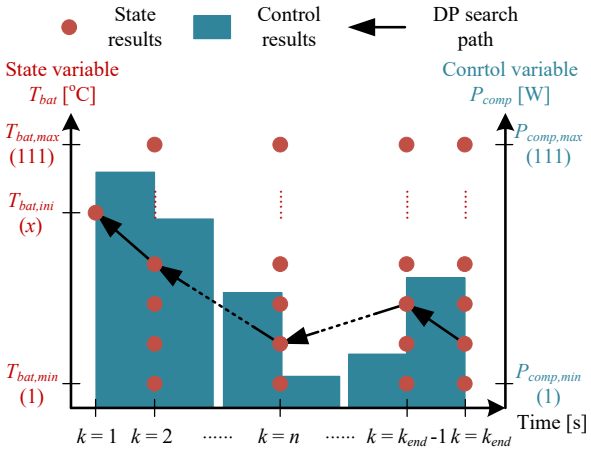

Figure 6: Principle of DP search procedure.

Battery cooling may result in reduced battery degradation but bring an increasing energy consumption. Thus the total cost including the battery capacity loss (aging) and the accumulated energy consumption for cooling under the entire driving cycle needs to be minimized by the DP, as shown below.

$$\text{Minimize}\Big[\sum_{k=1}^{k_{end}}\Big(\frac{Q_{bat}V_{bat}price_{bat}}{1000}\times\frac{\Delta Q_{loss,k}T_s}{0.2}+price_{ele}P_{cooling,k}T_s\Big)\Big], \tag{13}$$

where the first item is the battery capacity degradation cost, and the second item is the electricity cost associated with cooling the battery. Furthermore, $price_{bat}$ is the current battery price, i.e., 150USD/kWh [43], and the constant 0.2 denotes the maximum allowable battery capacity loss of 20% in EVs (the initial capacity of the battery pack is normalized to 1 [31]), $\Delta Q_{loss,k}$ is given in Eq. (5), $price_{ele}$ is the electricity price, i.e., 0.1USD/kWh, $P_{cooling,k}$ is mainly determined by $P_{comp,k}$, and T_s is set to 1s. This cost function is calculated considering 5 initial capacity losses 0.01% (a very small number that is close to 0 to avoid numerical issues and utilize the model successfully), 5%, 10%, 15%, and 20% to assess the average cost over the entire battery life [29]. The constraints involved in the DP optimization are given below:

$$\begin{cases} 0 \le P_{comp} \le 4500\text{W} \\ T_{bat,target} = 25^{\circ}\text{C} \\ I_{bat,min} \le I_{bat} \le I_{bat,max} \\ SoC_{bat,min} \le SoC_{bat} \le SoC_{bat,max} \end{cases} \tag{14}$$

for the second constraint, when the battery temperature is lower than or equal to 25°C, the searching range of P_{comp} will be modified to [0, 0].

3.2. Analysis of dynamic programming results

This study investigates three representative driving cycles, i.e., NYCC, SC03, and US06, representing typical urban, suburban, and highway conditions, respectively. As shown in Fig. 7 (a), the three driving cycles have the same time duration of 600s, with average velocities of 11.40km/h, 34.58km/h, and 77.36km/h and average distances of 1.90km, 5.76km, and 12.89km, respectively. Fig. 7 (b) shows the driving power demand P_d calculated based on the EV dynamic model.

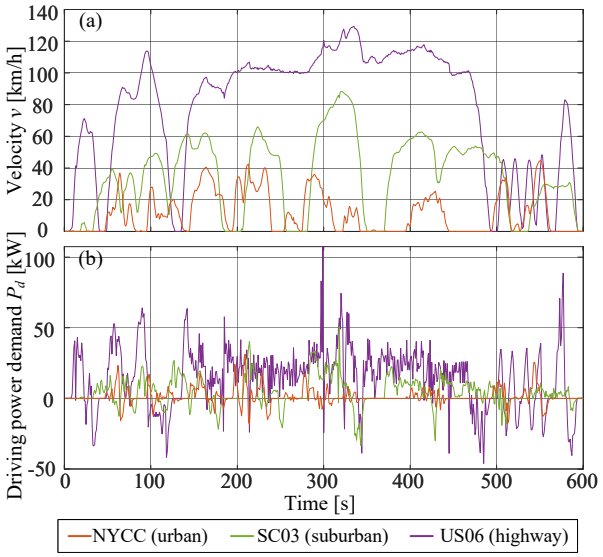

Figure 7: Three representative driving cycles: NYCC for urban, SC03 for suburban, and US06 for highway. (a) velocity, and (b) power demand.

The initial battery SoC is 95%, thus the DP is performed on the repeated driving cycles to consume the battery until its SoC is below 10%. Due to the different distances, NYCC is repeated 165 times, while SC03 and US06 are

repeated 55 and 18 times, respectively, leading to the total distances of 314km, 317km, and 232km for those three driving cycles.

Taking SC03 as an example (the detailed DP results of NYCC and US06 are not given in this section due to the limitation of the article length), the results of compressor power, battery heat generation/cooling rate, and battery/coolant temperatures are illustrated in Fig. 8. The whole battery cooling process can be divided into three stages: the fast cooling stage from 0s to 585s, the slow cooling stage from 586s to 2578s, and the temperature-maintaining stage from 2579s to the end.

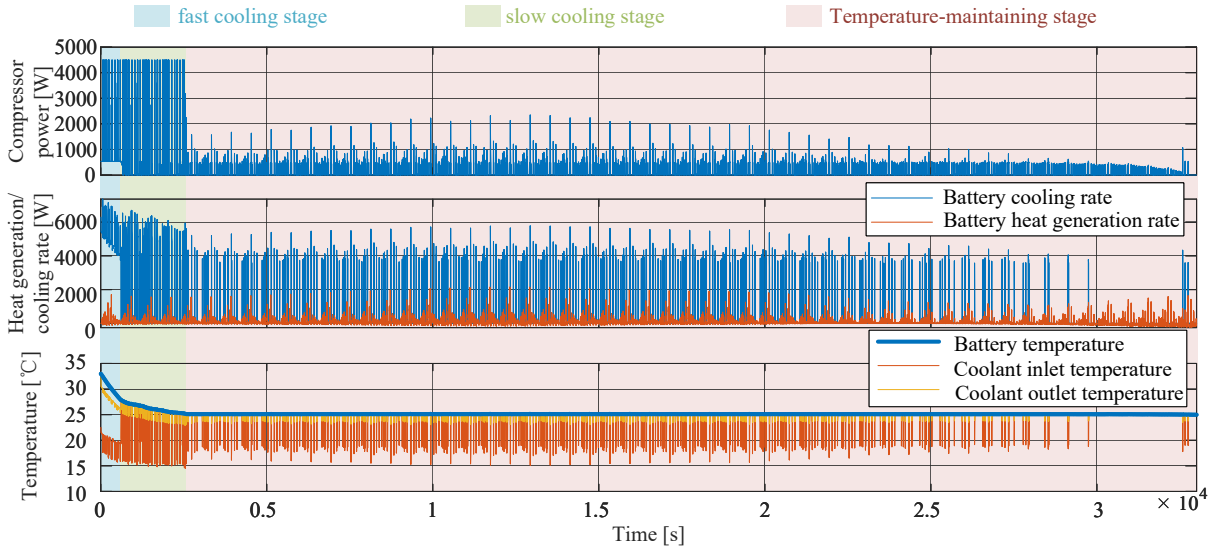

Figure 8: Offline DP results of compressor power, battery heating/cooling rate, and temperature under 55 SC03 driving cycles (33000s).

Specifically, in the fast cooling stage, the compressor is always working with P_{comp} between 500W and 4500W. At the end of fast cooling, the battery temperature is about 28°C. In this stage, the average coolant inlet temperature is 10°C lower than the battery temperature, and the average coolant outlet temperature is 2.25°C lower than the battery temperature. In the slow cooling stage, the compressor will not continuously work, while the compressor power can still reach the maximum value of 4500W. At about 2578s, the battery temperature drops to about 25°C. In the slow cooling and temperature-maintaining stages, the temperatures of coolant at the inlet and outlet can be equal to battery temperature sometimes, since the compressor only works intermittently. When the compressor doesn't work, the temperatures of coolant at the inlet and outlet will gradually increase through heat exchange with the battery. For the fast cooling stage, the temperatures of coolant at the inlet and outlet are always lower than the battery with continuous compressor operation. When it goes into the temperature-maintaining stage, the compressor power is between 0 and a low value to maintain the battery temperature around 25°C. Note that the compressor power during [10000, 15000s] is higher since the reversible entropy heat term is positive and higher when discharging (battery SoC is around 0.6 [31]). When battery SoC is less than 0.1, the reversible entropy heat is negative when discharging and can be higher than the resistance joule heat, for example, the compressor rarely works after 30000s.

4. Online battery cooling strategy

In this section, an online rule-based battery cooling strategy is proposed according to the DP results to achieve near-optimal performance with a low computational cost for practical implementations. To explore how DP balances the energy consumption and battery degradation in the cooling process, we carefully analyze the DP results, especially the underlying insights, i.e., the relationship between the traction power P_d and the compressor power P_{comp} under different stages. Specifically, as shown in Fig. 9 (a), in the fast cooling stage, the compressor is always cooling effectively ($>$ 500W). When the EV is in traction mode ($P_d > 0$), the compressor power is mainly

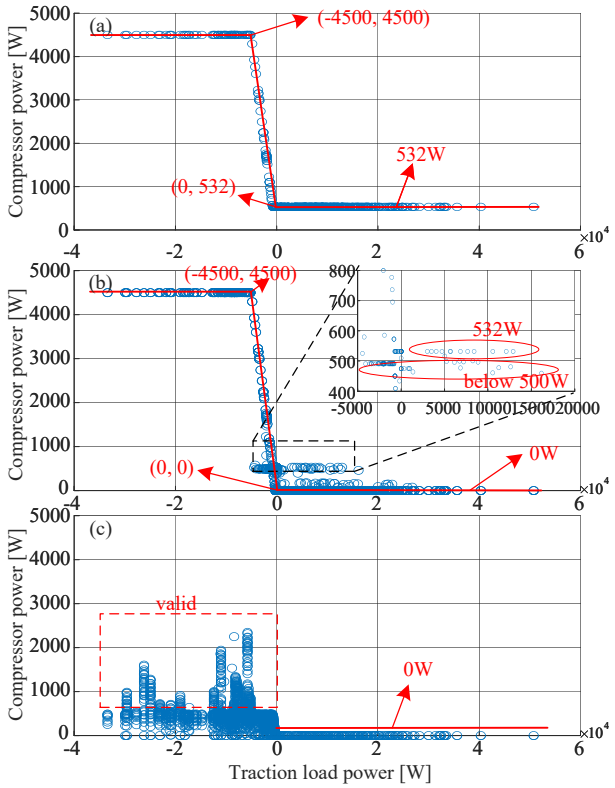

Figure 9: Optimal rules from the relationship between the compressor power P_{comp} and traction power P_d in DP results under SC03. (a) is the fast cooling stage, (b) is the slow cooling stage, and (c) is the temperature-maintaining stage.

constant at about 532W. When the EV is in regenerative braking mode ($P_d < 0$), the compressor power equals the regenerative power, and the part that exceeds 4500W is limited and used for charging the battery. As a result, the battery degradation can be remarkably reduced, as charging, especially at a high rate, will degrade the battery fast.

As shown in Fig. 9 (b), in the slow cooling stage, when the EV is in regenerative braking mode ($P_d < 0$), the cooling rule remains the same as in the fast cooling stage. However, when the EV is in traction mode ($P_d > 0$), the compressor does not work with P_{comp} concentrating around 0 W, meaning that all compressor power comes from the regenerative braking power. Note that even though there are a few points around 500W due to DP grid interpolation in the forward execution, most of them are below 500W and therefore negligible. As shown in Fig. 9 (c), in the temperature-maintaining stage, the compressor does not work ($P_{comp} = 0$) when the EV is in traction mode ($P_d > 0$). In regenerative braking mode, the compressor can hardly work at its maximum power of 4500W, and the points above 500W do not show a clear pattern. Despite this, the battery temperature will be maintained at around 25°C, fluctuating in a small range of about 0.1°C. Note that it is hard to execute different cooling rules between P_{comp} and T_{bat} in practice within 0.1°C. Therefore, all these valid points will be ignored for easy implementation, i.e., $P_{comp} = 0$. When the battery temperature rises, the BTMS can switch back to the slow cooling stage and cool the battery. Finally, three cooling rules can be extracted for the three cooling stages, and switching conditions based on the battery temperature are added according to the DP results, as illustrated in Fig. 10. Note that DP also behaves similarly under NYCC and US06, all key parameters of the rule-based battery cooling strategy under NYCC, SC03, and US06 are listed in Table 5.

For the three different driving cycles, only T_{sw1} is different, as high velocity will induce more heat generation in batteries, thereby requiring a longer fast cooling stage and a lower T_{sw1}. All T_{sw1} and T_{sw2} values are integers for ease of implementation, i.e., fractional digits are ignored. Here we can investigate why the battery cooling process is separated into fast and slow cooling stages by DP. The reason is that T_{sw1} is a temperature threshold related to the driving conditions, i.e., when $T_{bat} > T_{sw1}$, the low cooling power P_{low} can bring about a battery degradation cost

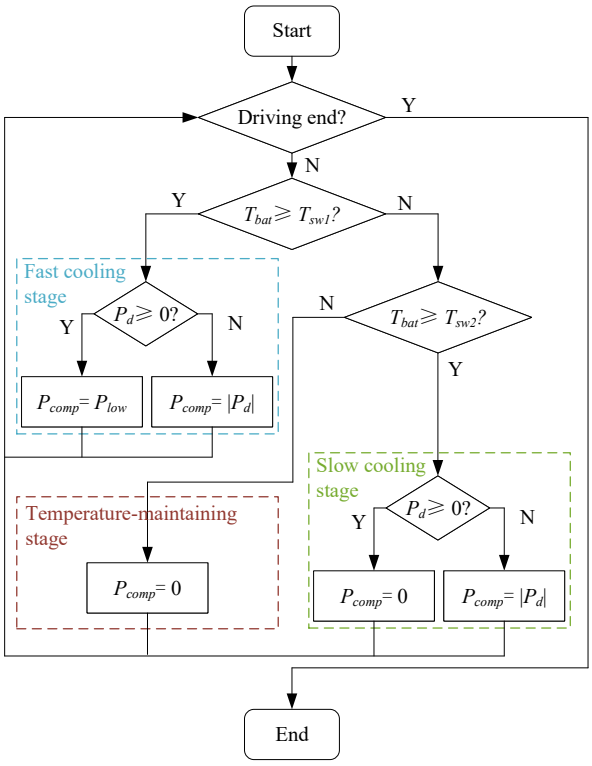

Figure 10: Flow chart of the online near-optimal rule-based battery cooling strategy.

Table 5: Parameters of the proposed rule-based battery cooling strategy.

Parameter	T_{sw1} (°C)	T_{sw2} (°C)	P_{low} (W)
NYCC	31	25	532
SC03	28	25	532
US06	26	25	532

reduction that is higher than electricity cost incurred by cooling, while when $T_{bat} < T_{sw1}$, the battery degradation cost reduction is less than the cooling electricity cost, as indicated in the optimal P_{comp} lookup table of DP. In Table 5, NYCC necessitates the highest T_{sw1}, while US06 requires the lowest, for the reason that higher vehicle speeds result in higher average traction power P_d. As a result, the proportion of additional cooling power P_{low} to traction power P_d decreases, and the proportion of additional battery degradation from P_{low} to the total power decreases as well. Therefore, a lower temperature threshold T_{sw1} is desired. In Fig. 7 (b), the average traction power P_d of NYCC, SC03, and US06 is 1.30, 4.43, and 14.56kW, respectively.

5. Results and Discussions

In this section, the proposed online cooling strategy is first compared with the offline DP, existing MPC, and BTMS off (no-cooling) cases. Then, a study of how driving distance impacts the driving economy and battery degradation is conducted to investigate the superiority of the proposed cooling strategy under different driving scenarios. Finally, a sensitivity analysis of three parameters (environment temperature T_{air}, mass flow rate of the coolant $\dot{m}_{clnt}$, and heat transfer area between the battery and coolant A_{bat}) is conducted to verify the robustness of the cooling strategy, and recommendations of battery cooling under different conditions are provided.

5.1. Comparative results of battery cooling process

The proposed rule-based cooling strategy is compared with the offline DP and online MPC to validate its performance. For existing online optimization MPC methods [19–22, 26, 27], the battery degradation is not explicitly minimized, we design the following cost function for the MPC, which is consistent with the above literature, as given by

$$minJ = \sum_{t=k}^{k+N_p-1} [\alpha(T_{bat} - T_{bat,target})^2 + price_{ele} P_{cooling,k} T_s], \quad k = 0, 1, 2, ... \tag{15}$$

where N_p is the prediction horizon of the MPC, α is the weighting factor of the temperature tracking term, and the second term of the cost function is the battery cooling cost which is the same as DP. The prediction horizon is 10, and a perfect prediction of EV velocity/traction load power (no prediction error) is considered. Note that such prediction is almost impossible in real-world implementations; thus, the MPC performance will deteriorate [28].

The battery capacity loss, battery SoC, and battery temperature results under NYCC, SC03, and US06 are presented in Fig. 11, as marked with different colors. The proposed rule-based cooling strategy consists of three stages: fast cooling, slow cooling, and temperature maintenance, for each driving cycle. As shown in Fig. 11 (a) and (b), the performance of the rule-based strategy is similar to that of DP, as demonstrated by the similarity in battery capacity loss and SoC values. In contrast, MPC has the highest battery capacity loss and lowest battery SoC under different driving cycles, despite consuming more cooling energy. As indicated in Fig. 11 (c), the final battery temperatures can be well maintained around 25°C by all three cooling methods. However, the enlarged figure shows that the cooling process of the proposed rule-based strategy is also similar to that of DP (almost overlap), while MPC cools the batter very fast (P_{comp} is around 3200W and T_{bat} reaches 25°C before 1300s for all three driving cycles) and then stops cooling until the battery temperature rises, causing a jagged temperature curve of MPC in the temperature-maintaining stage.

Table 6: Numerical comparison results of the proposed online strategy, DP method, MPC, and BTMS Off case.

Driving cycle	Method	Battery capacity loss (%)	Final battery SoC	Final battery temperature (°C)	Fast cooling period (s)	Slow cooling period (s)
NYCC (urban)	DP	0.0367	0.0458	24.9249	[0, 216]	[217, 4867]
	Rule	0.0375	0.0868	25.0381	[0, 224]	[225, 3561]
	MPC	0.0384	0.0541	24.7665	[0, 1295]	-
	BTMS Off	0.0476	0.1092	37.3083	-	-
SC03 (suburban)	DP	0.0322	0.0589	24.9831	[0, 585]	[586, 2578]
	Rule	0.0324	0.0666	25.0301	[0, 599]	[600, 2464]
	MPC	0.0333	0.0565	24.8184	[0, 959]	-
	BTMS Off	0.0411	0.0884	37.5637	-	-
US06 (highway)	DP	0.0380	0.0302	25.0077	[0, 927]	[928, 1770]
	Rule	0.0380	0.0254	25.0975	[0, 925]	[926, 1712]
	MPC	0.0392	0.0196	24.9323	[0, 850]	-
	BTMS Off	0.0487	0.0536	39.4827	-	-

A numerical comparison between the proposed rule-based strategy, DP method, MPC, and no-cooling (as a benchmark) cases is provided, as summarized in Table 6. For battery capacity loss, the proposed rule-based strategy achieves near-optimal performance with only a 2.18% increase in battery capacity loss compared to DP. Note that the rule-based strategy has the same final battery capacity loss as DP under US06, i.e., 0.0380, while it uses more battery energy. When compared with MPC, the proposed strategy reduces battery degradation by 2.34∼3.06% and saves 0.58∼3.27% consumed SoC. When compared with the no-cooling case, the proposed strategy reduces battery degradation by 21.22%, 21.17%, and 21.97% under NYCC, SC03, and US06, respectively, while the battery SoC only reduces by 2.24, 2.18, and 2.82, respectively (the consumed SoC is 2.66%/2.53%/3.15% more than the no-cooling case under NYCC/SC03/US06). Since the increased energy consumption is minor, the driving range of EVs is barely reduced.

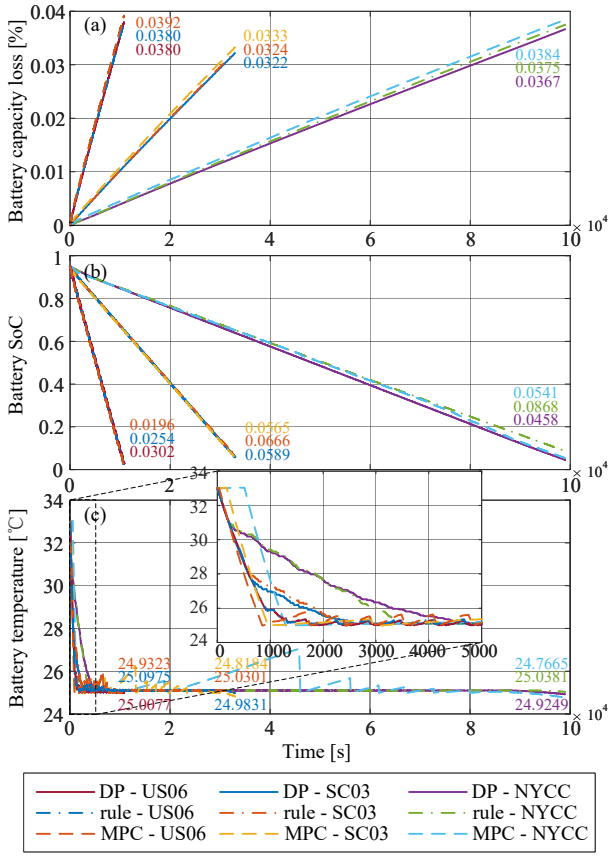

Figure 11: Comparison results of DP, MPC, and the proposed strategy in terms of (a) battery capacity loss, (b) battery SoC, and (c) battery temperature under different driving conditions.

5.2. Comparative results of driving economy and battery life

The impact of BTMS on the driving economy under different driving distances is further quantified in this section. Fig. 12 presents the detailed driving economy results of DP, rule-based strategy, MPC, and the no-cooling case with different driving cycle numbers. Although the reductions of total cost and battery degradation cost are not very significant when the driving cycle number is 1 (i.e., short trips), DP and rule-based strategy still provide a lower total cost because of the reduced battery degradation, meaning that it is worth cooling the battery even for short trips. Since the battery cooling cost reduces over time, battery cooling becomes increasingly necessary over a longer trip, when compared to the no-cooling strategy, as the accumulated reduction of battery degradation is significant. In addition, as shown in Fig. 12, the proposed rule-based strategy achieves similar results when compared to DP regarding the battery capacity loss cost, battery cooling cost, and total cost. The results are almost overlapped, indicating that the rule-based strategy can mimic DP very well under different types of driving cycles. It can be found that regardless of the adopted cooling strategy, cooling down the battery can reduce both the battery capacity loss cost and the total cost when compared to the no-cooling case. However, the MPC suffers from significantly higher driving costs at the beginning (i.e., the first 6/3/1 driving cycles under NYCC/SC03/US06), which means the MPC is not cost-effective for short-term driving. Note that in real-world applications, the prediction uncertainties can further deteriorate the MPC performance.

The battery life extension results under different cooling strategies, driving conditions, and distances are presented in Fig. 13. The proposed rule-based strategy is quite close to DP since both can extend the battery life from the beginning. As the battery temperature stabilizes, an approximately 20% battery life extension can be achieved. In contrast, due to the lack of long-term prediction information and the limitation of local optimization, the MPC cooling method will shorten the battery life for short-term driving. This highlights the superiority of the

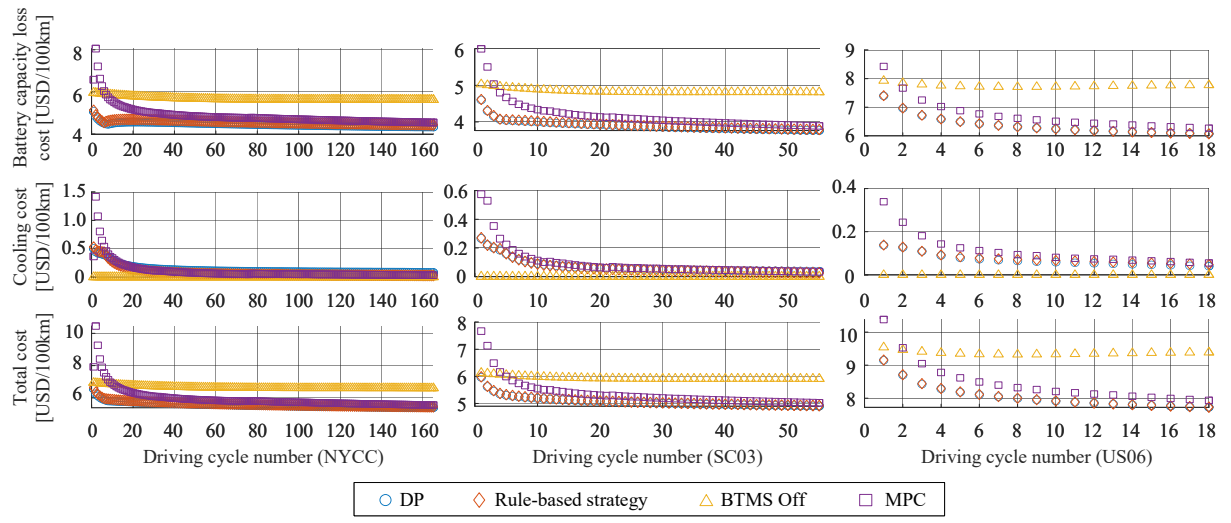

Figure 12: Economy comparison of DP, rule-based strategy, MPC, and BTMS Off cases under different driving conditions and different driving cycle numbers (NYCC, SC03, and US06).

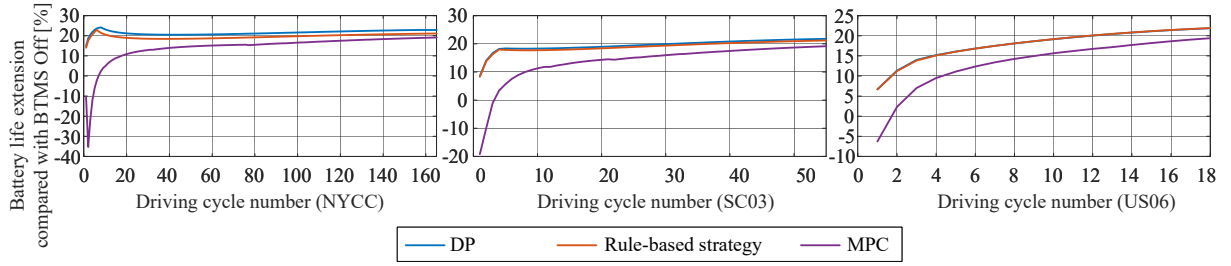

Figure 13: Battery life extension (compared with BTMS off) of DP, rule-based strategy, and MPC cases with different driving cycle numbers under different driving conditions (NYCC, SC03, and US06).

proposed method, which leverages the regenerative power to cool the battery, thereby prolonging battery life even in the battery cooling process.

An interesting phenomenon in Fig. 13 is that for DP and rule-based strategies, as the driving cycle number increases, the battery life extension increases first and then decreases under NYCC (i.e., urban driving condition), while for SC03 (i.e., suburban driving condition), such a phenomenon is much less obvious, and the battery life extension result is monotonic for US06 (i.e., highway driving condition). Specifically, at the beginning of urban driving conditions, the battery life extension mainly comes from the reduction of accumulated charging current, rather than the temperature reduction, as most regenerative braking energy is utilized to cool the battery. When the BTMS enters the temperature-maintaining stage, the charging process is more frequent during regenerative braking since the compressor power is around 0. As a result, although the battery temperature is reduced to 25°C, the battery degradation cost starts to increase. In contrast, under highway conditions, the battery life extension mainly comes from the temperature reduction, not the reduced battery charging current, as there are no aggressive and frequent braking actions. Thus, after the BTMS enters the temperature-maintaining stage (driving cycle number of 3 for DP and rule-based strategy, see the 1771s and 1712s in Table 6), the battery capacity loss cost can still decrease. The suburban driving condition stays somewhere between the above two driving conditions; therefore, the non-monotonic phenomena in the battery life extension still exist but is less pronounced. Note that the conclusions are based on the assumption that no temperature distribution and no core-surface temperature difference for the battery pack. In practice, the core temperature of the battery can be significantly higher than the surface [44] and has slower dynamics. Thus under higher core temperature, the battery pack has faster capacity degradation with

the same current, which means the effect of battery current on aging has been underestimated. During the real battery cooling process (till 25°C), reducing the battery charging (braking) current may have a greater impact than the temperature reduction on suppressing battery aging.

5.3. Parameter sensitivity analysis

In addition to the tested parameters of the battery cooling (i.e., T_{air} = 33°C, $\dot{m}_{clnt}$=0.18kg/s, and A_{bat}=3.1m^2), it is necessary to study other parameter values to assess the robustness of the proposed cooling strategy, as various cooling systems can be adopted in EVs. Given that the control-oriented model of the BTMS (Eq. (9)) is valid within the T_{air} range of 26∼40°C and the $\dot{m}_{clnt}$ range of 0.144∼0.216kg/s, we compare the following 6 parameter combinations in DP optimization, as listed in Table 7. Compared with Case 1, Cases 2, 3, and 4 are conducted to investigate different temperature conditions, and Cases 5 and 6 are set to examine the results of different BTMS designs, e.g., with a worse or better cooling capability.

Table 7: Six parameter combinations of T_{air}, A_{bat}, and $\dot{m}_{clnt}$

Case	T_{air} (°C)	$\dot{m}_{clnt}$ (kg/s)	A_{bat} (m^2)	Note
Case 1	33	0.180	3.1	benchmark
Case 2	28	0.180	3.1	lower environment temperature
Case 3	38	0.180	3.1	higher environment temperature
Case 4	40	0.180	3.1	higher environment temperature
Case 5	33	0.144	2.1	worse BTMS cooling capability
Case 6	33	0.216	4.1	better BTMS cooling capability

In Fig. 14, the battery temperature variation and battery capacity loss results of one driving cycle (600s) under the 6 parameter combinations are presented. Taking the NYCC (Fig. 14 (a, b)) as an example, it can be found that the battery capacity loss is mainly determined by T_{air} (average battery temperature), rather than A_{bat} and $\dot{m}_{clnt}$. Compared with Case 1/5/6, Case 3/4 has higher final battery temperatures (about 1.15∼3.12°C) and therefore higher final battery capacity losses (about 15.79∼24.61%), which also verifies the necessity of battery cooling in hot weather. BTMS parameters (A_{bat} and $\dot{m}_{clnt}$) have a more limited impact on battery cooling, e.g., the battery temperature and capacity loss results of Cases 1, 5, and 6 are close, even though the cooling process of Case 5 is slower and the one of Case 6 is faster.

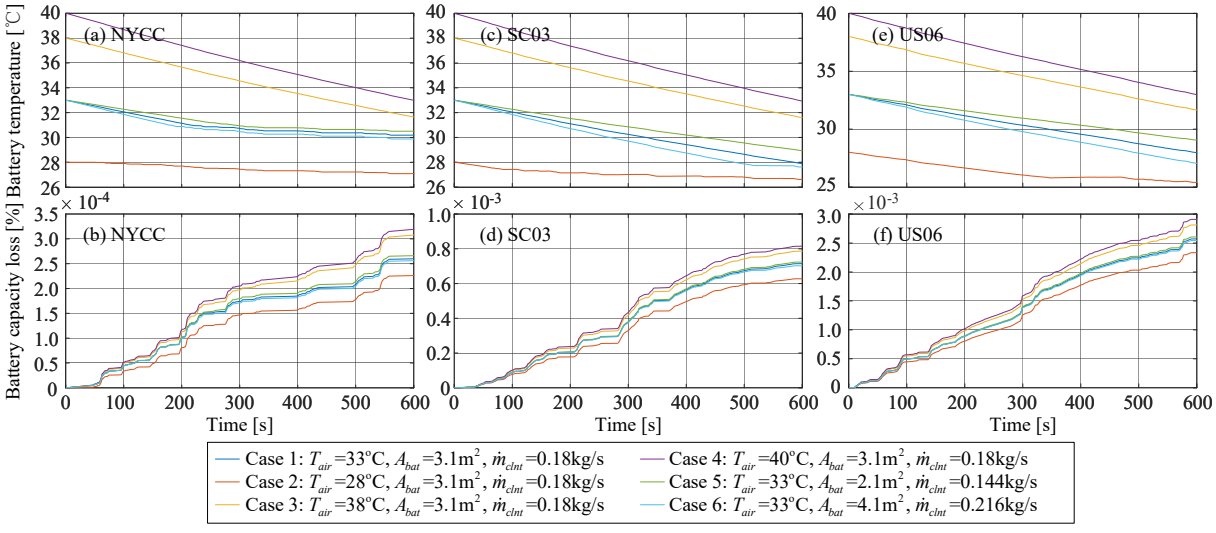

Figure 14: Cooling process of one driving cycle under different T_{air}, $\dot{m}_{clnt}$, and A_{bat} parameter combinations. (a, c, e) for battery temperature under NYCC, SC03, and US06. (b, d, f) for battery capacity loss under NYCC, SC03, and US06.

Results of SC03 and US06 are also similar: the battery capacity loss is mainly determined by T_{air} (average battery temperature), rather than A_{bat} and $\dot{m}_{clnt}$. However, the difference lies in the fact that for SC03 and US06, the final battery temperature difference between Cases 1, 5, and 6 is larger than that of NYCC. This is because the fast cooling stage of SC03 and US06 is much longer than NYCC (see Table 5), revealing that the BTMS parameters have a greater impact on the fast cooling stage (more heat exchange). To further investigate the effect of cooling parameters ($T_{air}/\dot{m}_{clnt}/A_{bat}$) on driving economy and battery degradation, the total cost reduction and battery degradation reduction compared with the no-cooling case are listed in Table 8. For different driving conditions, the short-trip and long-trip values denote the results of one driving cycle (600s) and the maximum driving cycle (165/55/18 for NYCC/SC03/US06), respectively.

Table 8: Total cost reduction and battery degradation reduction compared with the no-cooling case under different parameter combinations ($T_{air}/\dot{m}_{clnt}/A_{bat}$) and different driving cycles (NYCC/SC03/US06).

Index	Case	NYCC		SC03		US06	
		short-trip	long-trip	short-trip	long-trip	short-trip	long-trip
Total cost reduction (USD/100km)	Case 1	0.39	1.21	0.16	1.01	0.39	1.66
	Case 2	0.53	0.66	0.29	0.56	0.31	1.01
	Case 3	-0.06	1.81	0.27	1.51	0.55	2.36
	Case 4	0.01	2.05	0.33	1.70	0.62	2.65
	Case 5	0.23	1.21	0.10	1.01	0.30	1.65
	Case 6	0.48	1.21	0.26	1.01	0.47	1.67
Battery degradation reduction (%)	Case 1	14.95	22.90	8.54	21.76	6.71	21.89
	Case 2	17.15	14.47	10.24	13.65	5.97	14.86
	Case 3	9.73	30.41	9.65	29.10	7.78	28.21
	Case 4	10.30	32.92	10.21	31.55	8.33	30.37
	Case 5	12.91	22.96	7.39	21.80	5.46	21.89
	Case 6	16.21	22.85	10.15	21.75	7.69	21.90

The effect of $\dot{m}_{clnt}$ and A_{bat} can be found in Cases 1, 5, and 6 ($T_{air} = 33°C$). For different driving cycles, even though the total cost reduction and battery degradation reduction of Case 5 is lower than Case 1, and the total cost reduction and battery degradation reduction of Case 6 is higher than Case 1 under short-trip, the results will gradually converge as driving distance increases (long-trip). This also indicates that $\dot{m}_{clnt}$ and A_{bat} have limited impact on driving economy and battery degradation. Since for long-trip driving (enough time to cool T_{bat} to 25°C), T_{bat} can be well maintained with different $\dot{m}_{clnt}/A_{bat}$ parameters.

In contrast, the environment temperature T_{air} has a more significant effect on the driving economy and battery degradation. By comparing Cases 1, 2, 3, and 4, it can be found that higher temperatures lead to greater reductions in both total cost and battery degradation during long trips. However, for short trips in urban areas (600s, about 2km), battery cooling can increase the total cost in Case 3 or has no cost contribution in Case 4, even though the battery degradation is still reduced. This is because (1) the fast cooling process will take a longer time since the environmental temperature is high, and thus the cooling cost is higher than the reduced battery degradation cost, and (2) the cooling cost in short-term urban driving conditions is higher than that in suburban and highway conditions due to larger proportion of fast cooling power to total load power and the lower BTMS efficiency (see Eq. (10)). Note that when the driving cycle number is 2 (NYCC, 1200s, about 4km), there are only limited cost reductions of 0.63USD/100km and 0.69USD/100km for Cases 3 and 4. Due to this very limited cost reduction under short-trip urban driving, battery cooling is unnecessary. However, for long trips in hot weather, such as those experienced by Taxis [45], battery cooling is essential.

From the analysis above, it can be found that there is no significant difference in the driving economy and battery degradation under different cooling systems. Recommendations regarding battery cooling are then given as follows: (1) The driving economy is mainly influenced by the driving distance and environment temperature, and battery cooling is more necessary under long-trip driving and high environment temperature; (2) Battery cooling will provide more total cost reduction under higher temperature environment; and (3) Battery cooling is essential for long-trip driving regardless of the driving conditions.

6. Conclusion

This paper investigates the battery cooling optimization of passenger EVs in hot weather. An electrical-thermal-aging model for commercial $LiFePO_4$ batteries is adopted, and a control-oriented dynamic model of an onboard BTMS is established to characterize the relationship between the compressor power and the battery cooling rate under various operation conditions. Then the DP algorithm is introduced to simultaneously minimize the battery degradation cost and the battery cooling cost. By analyzing the DP results, an online near-optimal battery cooling strategy is proposed, which contains a fast cooling stage, a slow cooling stage, and a temperature-maintaining stage.

Simulation results under 33°C condition show that the proposed rule-based strategy can achieve very close performance when compared to DP, e.g., the battery degradation difference between the two strategies under urban/suburban/highway driving cycle is only 2.18%/0.62%/0% with 4.53%/0.86%/-0.52% less battery energy consumed. Compared with the existing MPC method, the proposed rule-based strategy can reduce battery degradation by 2.34∼3.06% and saves 0.58∼3.27% consumed battery energy. While compared with the no-cooling case, the proposed rule-based strategy reduces battery degradation by about 21% with only 2.66∼3.15% more battery energy consumed under different driving cycles.

Detailed comparison with existing MPC and no-cooling cases, parameter sensitivity analysis of environment temperature/BTMS design/driving distance, and cooling economy analysis are conducted under urban, suburban, and highway driving conditions. Results show that (1) The proposed rule-based cooling strategy can significantly reduce battery degradation without obviously reducing driving range; (2) Different BTMS parameters can influence the cooling speed but will not have a significant impact on driving economy; (3) Battery cooling provides better economy when the environment temperature increases and the trip becomes longer; (4) The proposed battery cooling method is cost-effective for all driving conditions only except for high-temperature short-term urban drivings. The key finding of this study is that using as much regenerative energy as possible to cool the battery pack can dramatically improve the driving economy and reduce battery degradation.

Acknowledgment

This work was supported in part by the National Natural Science Foundation of China (Grant No. 52272339) and Natural Science Foundation of Hunan Province (Grant No. 2021JJ30828), China Railway Signal and Communication Corporation Limited Research Project (Grant No. 2300-K1200035), and China Shenhua Heavy Freight Train Group Operation Control System Technology Project. The first author is supported by the China Scholarship Council.

Special thanks to the support by Magna PT Powertrain (Shanghai) Co., Ltd., for providing KULI technical service. Special thanks to Seho Park from the Pusan National University, South Korea for providing help with BTMS modeling, and Jiahao Huang from Huawei Technologies Co., Ltd., China for providing assistance with software.

Appendix: BTMS orthogonal experiment and model parameters

To develop a BTMS model from the orthogonal experiment, this paper selects an onboard air-conditioning system officially supplied by Magna, and this model is built into KULI software which is well validated by experiments [38, 39]. In this model, R-134a is adopted as the refrigerant for the air-conditioning loop, and 50% ethylene glycol-water mixture is selected as the coolant for cooling the battery pack. According to existing studies [36, 37], the inlet temperature of the condenser, the air mass flow rate of the condenser, the outlet temperature of the battery coolant, the mass flow rate of coolant, and the rotation speed of the compressor are chosen as the main parameters to design the orthogonal experiment. To simplify the complex model, the following assumptions are adopted.

1. The cooling fan for enhancing heat exchange is set to supply a constant air mass flow.
2. All cooling capacity is used for the battery pack, i.e., the impact of the EV cabin is not taken into account.

Therefore, experiment variables include the outlet temperature of coolant $T_{clnt,out}$, volumetric flow rate of coolant $\dot{q}_{clnt}$, ambient air temperature T_{air}, vehicle speed v (affects inlet air mass flow rate of condenser, the total

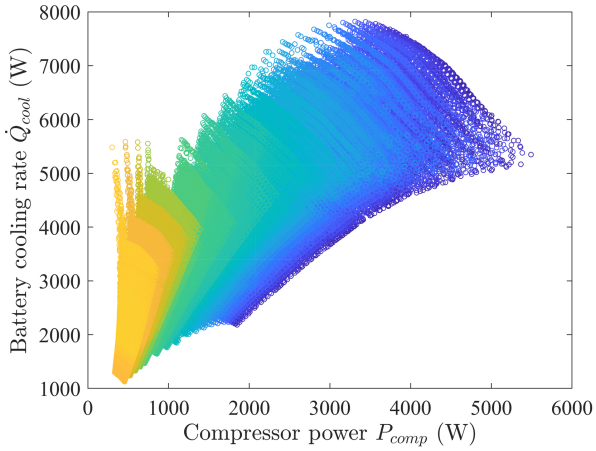

Figure A: Simulation results: relationship between cooling rate $\dot{Q}_{cool}$ and compressor power P_{comp}.

air mass flow $\dot{m}_{air}$ consists of air supplied by the EV velocity and fan), and electrical power of the compressor P_{comp}. The target variable is set as battery cooling rate $\dot{Q}_{cool}$. See Table 3.

The relationship between the cooling rate and compressor power in the experiment is shown in Fig. A. Note that it is almost impossible to fit a high-precision and accurate correlation formula with all data directly. Therefore, we divide data into regions and then fit them sequentially, where T_{air} and $\dot{q}_{clnt}$ are selected as division basis. The BTMS model (Eq. (9)) comprehensively considered compressor electrical power, ambient temperature, the outlet temperature of the coolant, air mass flow rate, and mass flow rate of the coolant. Detailed data of the six coefficients, i.e., Fig. 4, is attached.

References

[1] X. Feng, M. Ouyang, X. Liu, L. Lu, Y. Xia, X. He, Thermal runaway mechanism of lithium ion battery for electric vehicles: A review, Energy Storage Materials 10 (2018) 246–267.

[2] Y. Deng, C. Feng, E. Jiaqiang, H. Zhu, J. Chen, M. Wen, H. Yin, Effects of different coolants and cooling strategies on the cooling performance of the power lithium ion battery system: A review, Applied Thermal Engineering 142 (2018) 10–29.

[3] A. H. Akinlabi, D. Solyali, Configuration, design, and optimization of air-cooled battery thermal management system for electric vehicles: A review, Renewable and Sustainable Energy Reviews 125 (2020) 109815.

[4] V. Mali, R. Saxena, K. Kumar, A. Kalam, B. Tripathi, Review on battery thermal management systems for energy-efficient electric vehicles, Renewable and Sustainable Energy Reviews 151 (2021) 111611.

[5] K. Chen, S. Wang, M. Song, L. Chen, Configuration optimization of battery pack in parallel air-cooled battery thermal management system using an optimization strategy, Applied Thermal Engineering 123 (2017) 177–186.

[6] Y. Mu, K. Gao, P. Luo, D. Ma, H. Chang, R. Du, Research on bionic fish scale channel for optimizing thermal performance of liquid cooling battery thermal management system, Batteries 9 (2) (2023).

[7] H. Dai, B. Jiang, X. Hu, X. Lin, X. Wei, M. Pecht, Advanced battery management strategies for a sustainable energy future: Multilayer design concepts and research trends, Renewable and Sustainable Energy Reviews 138 (2021) 110480.

[8] N. Ghaeminezhad, Z. Wang, Q. Ouyang, A review on lithium-ion battery thermal management system techniques: A control-oriented analysis, Applied Thermal Engineering (2022) 119497.

[9] J. Kim, J. Oh, H. Lee, Review on battery thermal management system for electric vehicles, Applied Thermal Engineering 149 (2019) 192–212.

[10] M. Wang, S. Teng, H. Xi, Y. Li, Cooling performance optimization of air-cooled battery thermal management system, Applied Thermal Engineering 195 (2021) 117242.

[11] S. Lee, Y. Chung, S. Kim, Y. Jeong, M. S. Kim, Investigation on the performance enhancement of electric vehicle thermal management system utilizing floating loop with finite heat exchanger size, Energy Conversion and Management 255 (2022) 115265.

[12] Y. Wang, G. Zhang, X. Yang, Optimization of liquid cooling technology for cylindrical power battery module, Applied Thermal Engineering 162 (2019) 114200.

[13] C. Yang, H. Xi, M. Wang, Structure optimization of air cooling battery thermal management system based on lithium-ion battery, Journal of Energy Storage 59 (2023) 106538.

[14] M. Lu, X. Zhang, J. Ji, X. Xu, Y. Zhang, Research progress on power battery cooling technology for electric vehicles, Journal of Energy Storage 27 (2020) 101155.

[15] X. Hu, Y. Zheng, X. Lin, Y. Xie, Optimal multistage charging of nca/graphite lithium-ion batteries based on electrothermal-aging dynamics, IEEE Transactions on Transportation Electrification 6 (2) (2020) 427–438.

[16] J. Wang, P. Liu, J. Hicks-Garner, E. Sherman, S. Soukiazian, M. Verbrugge, H. Tataria, J. Musser, P. Finamore, Cycle-life model for graphite-lifepo4 cells, Journal of Power Sources 196 (8) (2011) 3942–3948.

[17] M. A. Jeffers, L. Chaney, J. P. Rugh, Climate control load reduction strategies for electric drive vehicles in cold weather, SAE International Journal of Passenger Cars-Mechanical Systems 9 (2016-01-0262) (2016) 75–82.

[18] X. Hu, Y. Zheng, D. A. Howey, H. Perez, A. Foley, M. Pecht, Battery warm-up methodologies at subzero temperatures for automotive applications: Recent advances and perspectives, Progress in Energy and Combustion Science 77 (2020) 100806.

[19] M. R. Amini, I. Kolmanovsky, J. Sun, Hierarchical mpc for robust eco-cooling of connected and automated vehicles and its application to electric vehicle battery thermal management, IEEE Transactions on Control Systems Technology 29 (1) (2020) 316–328.

[20] M. R. Amini, H. Wang, X. Gong, D. Liao-McPherson, I. Kolmanovsky, J. Sun, Cabin and battery thermal management of connected and automated hevs for improved energy efficiency using hierarchical model predictive control, IEEE Transactions on Control Systems Technology 28 (5) (2019) 1711–1726.

[21] S. Zhao, C. C. Mi, A two-stage real-time optimized ev battery cooling control based on hierarchical and iterative dynamic programming and mpc, IEEE Transactions on Intelligent Transportation Systems (2021).

[22] S. Park, C. Ahn, Computationally efficient stochastic model predictive controller for battery thermal management of electric vehicle, IEEE Transactions on Vehicular Technology 69 (8) (2020) 8407–8419.

[23] X. Kuang, K. Li, Y. Xie, C. Wu, P. Wang, X. Wang, C. Fu, Research on control strategy for a battery thermal management system for electric vehicles based on secondary loop cooling, IEEE Access 8 (2020) 73475–73493.

[24] S. Bauer, A. Suchaneck, F. P. León, Thermal and energy battery management optimization in electric vehicles using pontryagin's maximum principle, Journal of Power Sources 246 (2014) 808–818.

[25] Y. Zhao, D. Dan, S. Zheng, M. Wei, Y. Xie, A two-stage eco-cooling control strategy for electric vehicle thermal management system considering multi-source information fusion, Energy (2023) 126606.

[26] S. Park, C. Ahn, Model predictive control with stochastically approximated cost-to-go for battery cooling system of electric vehicles, IEEE Transactions on Vehicular Technology 70 (5) (2021) 4312–4323.

[27] Y. Xie, C. Wang, X. Hu, X. Lin, Y. Zhang, W. Li, An mpc-based control strategy for electric vehicle battery cooling considering energy saving and battery lifespan, IEEE Transactions on Vehicular Technology 69 (12) (2020) 14657–14673.

[28] Y. Wu, Z. Huang, Y. Zheng, Y. Liu, H. Li, Y. Che, J. Peng, R. Teodorescu, Spatial–temporal data-driven full driving cycle prediction for optimal energy management of battery/supercapacitor electric vehicles, Energy Conversion and Management 277 (2023) 116619.

[29] Y. Wu, Z. Huang, H. Hofmann, Y. Liu, J. Huang, X. Hu, J. Peng, Z. Song, Hierarchical predictive control for electric vehicles with hybrid energy storage system under vehicle-following scenarios, Energy 251 (2022) 123774.

[30] Z. Song, X. Zhang, J. Li, H. Hofmann, M. Ouyang, J. Du, Component sizing optimization of plug-in hybrid electric vehicles with the hybrid energy storage system, Energy 144 (2018) 393–403.

[31] Z. Song, J. Li, X. Han, L. Xu, L. Lu, M. Ouyang, H. Hofmann, Multi-objective optimization of a semi-active battery/supercapacitor energy storage system for electric vehicles, Applied Energy 135 (2014) 212–224.

[32] J. Huang, Z. Huang, Y. Wu, Y. Liu, H. Li, F. Jiang, J. Peng, Sizing optimization research considering mass effect of hybrid energy storage system in electric vehicles, Journal of Energy Storage 48 (2022) 103892.

[33] Z. Song, H. Hofmann, J. Li, X. Han, M. Ouyang, Optimization for a hybrid energy storage system in electric vehicles using dynamic programing approach, Applied Energy 139 (2015) 151–162.

[34] Z. Song, H. Hofmann, J. Li, J. Hou, X. Zhang, M. Ouyang, The optimization of a hybrid energy storage system at subzero temperatures: Energy management strategy design and battery heating requirement analysis, Applied Energy 159 (2015) 576–588.

[35] Y. Liu, Z. Huang, Y. Wu, L. Yan, F. Jiang, J. Peng, An online hybrid estimation method for core temperature of lithium-ion battery with model noise compensation, Applied Energy 327 (2022) 120037.

[36] C. Wang, B. Wang, M. Cui, F. Wei, Cooling seasonal performance of inverter air conditioner using model prediction control for demand response, Energy and Buildings 256 (2022) 111708.

[37] H. Wang, M. R. Amini, Q. Hu, I. Kolmanovsky, J. Sun, Eco-cooling control strategy for automotive air-conditioning system: Design and experimental validation, IEEE Transactions on Control Systems Technology 29 (6) (2020) 2339–2350.

[38] D. Li, C. Zhang, R. Fan, L. Xu, Y. Wang, W. Guo, J. Chen, M. Ni, An innovative thermal management method for cooling loop of electric driving system for durable and high efficiency electric vehicle, Applied Thermal Engineering 195 (2021) 117176.

[39] Z. Qi, J. Chen, Z. Chen, Analysis and simulation of mobile air conditioning system coupled with engine cooling system, Energy Conversion and Management 48 (4) (2007) 1176–1184.

[40] Y. Wang, W. Li, Z. Zhang, J. Shi, J. Chen, Performance evaluation and prediction for electric vehicle heat pump using machine learning method, Applied Thermal Engineering 159 (2019) 113901.

[41] G. Karimi, X. Li, Thermal management of lithium-ion batteries for electric vehicles, International Journal of Energy Research 37 (1) (2013) 13–24.

[42] R. Bellman, Dynamic programming, Science 153 (3731) (1966) 34–37.

[43] BloombergNEF., Hitting the ev inflection point., `https://www.bundestag.de/resource/blob/842494/ae21227aee8ae66277324a0abba943fc/Artikel-2-Jekaterina-Boening-data.pdf` (2021).

[44] Z. Song, N. Yang, X. Lin, F. P. Delgado, H. Hofmann, J. Sun, Progression of cell-to-cell variation within battery modules under different cooling structures, Applied Energy 312 (2022) 118836.

[45] J. Niu, W. Zhuang, J. Ye, Z. Song, G. Yin, Y. Zhang, Optimal sizing and learning-based energy management strategy of ncr/lto hybrid battery system for electric taxis, Energy 257 (2022) 124653.